The International Journal of Robotics Research

Uniform Coverage of Automotive Surface Patches

Prasad N. Atkar, Aaron Greenfield, David C. Conner, Howie Choset and Alfred A. Rizzi

The online version of this article can be found at:
http://ijr.sagepub.com/cgi/content/abstract/24/11/883

Additional services and information for *The International Journal of Robotics Research* can be found at:

Email Alerts: http://ijr.sagepub.com/cgi/alerts

Subscriptions: http://ijr.sagepub.com/subscriptions

Reprints: http://www.sagepub.com/journalsReprints.nav

Permissions: http://www.sagepub.com/journalsPermissions.nav

Prasad N. Atkar
Aaron Greenfield
David C. Conner
Howie Choset
Alfred A. Rizzi

Carnegie Mellon University
Pittsburgh, PA 15213, USA
choset@cs.cmu.edu

Uniform Coverage of Automotive Surface Patches

Abstract

In spray painting applications, it is essential to generate a spray gun trajectory such that the entire surface is completely covered and receives an acceptably uniform layer of paint deposition; we call this the "uniform coverage" problem. The uniform coverage problem is challenging because the atomizer emits a non-trivial paint distribution, thus making the relationships between the spray gun trajectory and the deposition uniformity complex. To understand the key issues involved in uniform coverage, we consider surface patches that are geodesically convex and topologically simple as representative of subsets of realistic automotive surfaces. In addition to ensuring uniform paint deposition on the surface, our goal is to also minimize the associated process cycle time and paint waste. Based on the relationships between the spray gun trajectory and the output characteristics (i.e., uniformity, cycle time and paint waste), our approach decomposes the coverage trajectory generation problem into three subproblems: (1) selecting a seed curve, (2) determining a speed profile along each pass, and (3) selecting the spacing between successive passes. Using concepts such as area magnification and the Gauss–Bonnet theorem from differential geometry, as well as standard optimization procedures, we present procedures to solve each subproblem independently from the others. We demonstrate our trajectory planning procedures by approximating real automotive surfaces by simple surfaces in simulation, and finally evaluate the effectiveness of our algorithms experimentally on real automotive surfaces.

KEY WORDS—uniform coverage, trajectory planning, spray painting, surface deposition

1. Introduction

Robots are widely used for spray painting in the automotive industry. Paint specialists typically program the robot manually and produce coverage paths based on their experience, often requiring three to five months to completely plan trajectories on a new automobile model (Jacob Braslaw, private communication). This programming time is a critical bottleneck in the "concept-to-consumer" timeline for bringing a new automobile to the market. Automating the process of trajectory planning will help the paint specialists reduce this programming time by offering them reasonable guidelines for effective paths. Moreover, automation of trajectory planning procedures will enable minimization of the cycle time and a reduction in paint waste, thus helping the paint specialists to produce more efficient paint application systems. In this work, we develop procedures for automated generation of end-effector trajectories to optimize robotic spray-painting output characteristics over simple surfaces. However, the methodologies described in this paper can also be applied to general material removal/deposition applications such as CNC machining or bone shaving.

To make the problem of trajectory generation more challenging, this work considers the use of electrostatic rotating bell (ESRB) atomizers (one of the most popular spray painting mechanisms) which emit paint distributions that are significantly complex. This complexity is further compounded by the surface geometry of non-planar automotive surfaces, where the paint distribution pattern "warps" depending on the surface curvature.

Taking the atomizer and the surface properties into consideration for automated trajectory generation requires a large multidimensional search-space. For example, a naive approach to trajectory generation that assumes that the trajectory is discretely represented by n trajectory points requires $7n$ variables (three each for spray gun position and orientation, and one for speed per trajectory point). Typically, in the automotive industry, the axis of the spray gun is held normal to

883

the surface to obtain uniform electrostatics effects. Also, paint specialists typically use constant speed trajectories. Therefore, with these constraints, the discretized representation of the trajectory with n points will require $4n$ variables (three for position, one for orientation for each trajectory point). Thus, the dimensionality of the search space of the discretized trajectory representation remains very large even after applying typical spray painting constraints.

Finally, the nature of the desired output characteristics themselves make automation of trajectory generation a challenging task. The material deposition process is typically multi-objective in the sense that it is desirable to minimize cycle time and paint waste, while obtaining an acceptable deposition uniformity (typically measured as normalized standard deviation of material deposition). These characteristics often lead to a conflicting set of criteria for trajectory generation and care must be taken to balance the overall cost trade-offs against these characteristics.

To make the optimization of coverage path parameters tractable, our approach relies on decomposing the uniform coverage problem into several subproblems that can be solved relatively independently (see Figure 1(a)). First, the geometrically and topologically complex automobile surface is segmented into "simple" patches, i.e., surfaces that are topologically simple (i.e., diffeomorphic to a disk with no holes) as well as geodesically convex[1] (see Figure 2). Next, on each simple surface patch, we generate trajectories by selecting a seed curve and repeatedly offsetting it sideways until the surface is covered completely (see Figure 1(b)). Thus, the trajectory generation problem on a simple patch is then reduced to the three relatively decoupled subproblems: (i) selection of a seed curve on the surface, (ii) selection of the speed profile along a given pass, and (iii) selection of the spacing between a given pass and its adjacent pass. Note that the seed curve (sometimes referred to as the start curve) is the first pass generated during the trajectory planning procedure, and is not, in general, the first pass traversed by the atomizer when it starts covering a given surface.

The selection of the seed curve impacts the spatial location and orientation as well as the number of the remaining passes in the coverage path, which, in turn, affect the uniformity of paint deposition and the overall cycle time. Thus, selecting the seed curve can be seen as determining a good "seed" point to start the coverage trajectory optimization procedure. Next, the uniformity of paint deposition can be seen as having two components: (i) uniformity along the direction of passes, and (ii) uniformity in the direction orthogonal to the passes. Optimization of the atomizer speed along the trajectory produces consistent paint profiles along a pass, thus improving
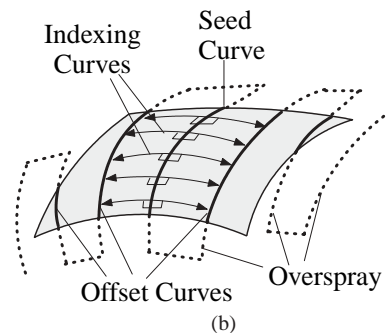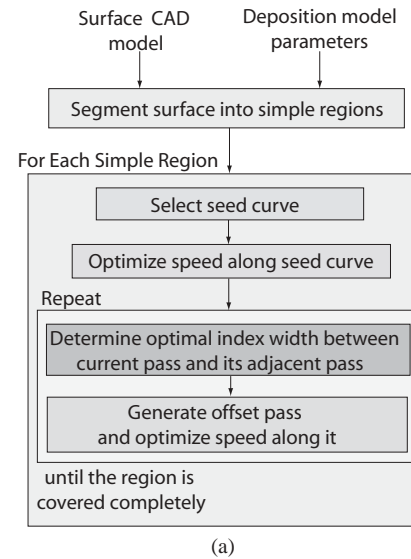

(a)

(b)

Fig. 1. (a) Algorithmic overview of our trajectory planning algorithm. (b) Our algorithm generates a coverage path on arbitrary simple surfaces by selecting a seed curve and offsetting it sideways within the surface to generate new passes.

uniformity in the direction along the passes (see Figure 3). To produce uniform paint deposition in the direction orthogonal to the passes, we optimize the spacing between passes, called the "index width", to overlap the paint profiles of two adjacent passes appropriately. Finally, we follow the industry norm of selecting the orientation of the atomizer normal to the surface. The effectiveness of our trajectory generation framework for simple patches lies in the fact that each of the three subproblems can be solved in a reasonable amount of time essentially independently from the others. This approach does not yield globally optimal solutions in general; however, it enables the user to obtain practical and effective atomizer trajectories quickly.

In this paper, we focus primarily on the development of automated trajectory generation tools for simple patches. Our work on surface segmentation is described in Atkar et al.

---

1. A surface S is geodesically convex if for any two points $p, q \in S$, the shortest path connecting the two points is a geodesic curve. Recall that a geodesic curve α has identically zero geodesic curvature, i.e., $\kappa_g[\alpha(t)] = \langle [\dot{\alpha}(t)]', J\dot{\alpha}(t) \rangle = 0$ for all t, where $J\dot{\alpha}(t)$ is the unit vector orthogonal to $\dot{\alpha}(t)$ lying in the tangent space at S.
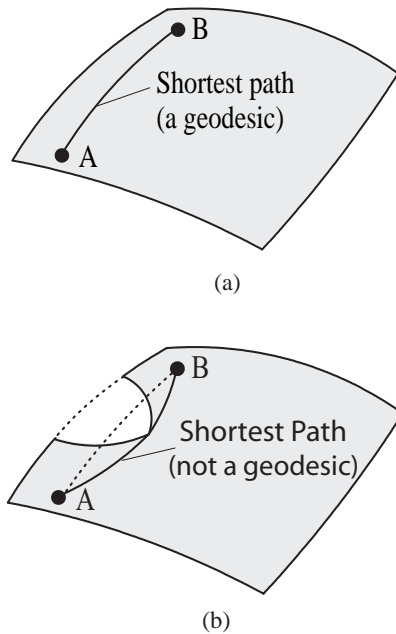
(a)

(b)

Fig. 2. (a) A geodesically convex bent sheet; here the shortest curve joining any two points is a geodesic. (b) The surface is not geodesically convex because the shortest curve in the surface joining two points A and B is not a geodesic.
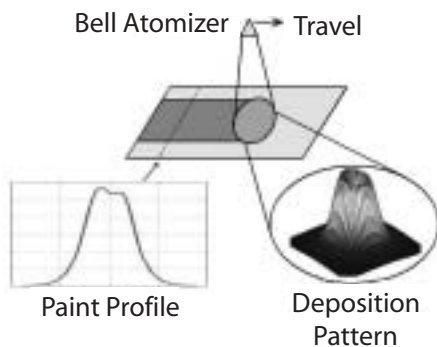

Fig. 3. A typical deposition model and the paint profile across the paint swath on a flat planar sheet.

(2005). Note that the effectiveness of any automated trajectory generation procedures depends heavily on reasonably accurate and fast paint deposition prediction on arbitrary surfaces; our prior work on deposition modeling addresses this issue (Conner et al. 2002, 2004).

This paper is organized as follows. We first review the relevant literature on trajectory planning for material deposition or removal applications in Section 2.1. Our prior work on deposition modeling is briefly discussed in Section 2.2.

We describe the procedures for seed curve selection in Section 3, whereas we formulate the speed optimization problem in Section 4. We address the index optimization problem in Section 5 for surfaces with increasing geometric complexity: planar surfaces, extruded sheets and surfaces with non-zero Gaussian curvature.[2] Finally, we demonstrate our coverage procedures for a variety of surfaces in simulation as well as experimentally in Section 6. We would like to emphasize that the effectiveness of our coverage procedures to optimize all output characteristics on real automobile surface can only be examined in the overall framework of trajectory generation, and in this work we make no such attempt. None the less, we are able to evaluate the effectiveness of our procedures to optimize uniformity (which in the most important output characteristic) on real automobile surfaces.

2. Prior Work

2.1. Related Work

Spray painting and CNC machining applications are conceptually similar in the sense that both these applications require the end-effector to uniformly traverse the target surface. Therefore, similar methodologies can be employed to automate path planning for these applications. For spray painting and CNC machining, most prior researchers typically focus on a particular subproblem for the trajectory generation procedure: seed curve selection, speed optimization, or index width optimization. However, only a few researchers have studied all the three problems simultaneously.

2.1.1. Seed Curve Selection

For seed curve selection, most prior researchers (Suh, Woo, and Noh 1991; Asakawa and Takeuchi 1997; Sahir and Balkan 2000; Sheng et al. 2000) select a pass orientation that aligns with one of the faces of a bounding box that surrounds the surface, while choosing the relative position (with respect to the surface boundary) of the seed curve arbitrarily. Such an approach to seed curve selection implicitly tries to minimize cycle time, but does not consider the effects of the relative position of the seed curve on paint uniformity and can lead to poor uniformity results. To minimize cycle time for direction-parallel CNC milling applications of planar surfaces, Held (1991) selects an appropriate orientation for passes to minimize the number of cells, thus minimizing the number of tool retractions and the number of turns in the coverage path. Similarly, Huang (2001) gives an approach for reducing the cycle time for coverage by minimizing the number of passes in the coverage path; however, this work is limited to planar problems. Kim and Sarma (2003) use vector fields to choose

2. The Gaussian curvature of a surface at a given point is the product of the principal curvatures of the surface at that point, i.e., $K = k_{min} \cdot k_{max}$. Gaussian curvature measures how much the surface bends in two orthogonal directions.

the pass orientation that minimizes the cycle time with an implicit constraint on deposition uniformity; however, they do not consider the effect of the vector field orientation on uniformity explicitly.

Smith et al. (2002) study the effect of the spatial orientation of the passes (and thus, that of a seed curve) on the surface finish of a machined surface. Their approach generates the coverage path by intersecting the target surface with a series of parallel equidistant planes, whose normal is maximally "away" from the normals to the surface. This maximally orthogonal section plane normal corresponds to the center of the largest circle inscribed in the complement of the symmetrized Gauss map of the target surface (see Figure 4). This approach to coverage path generation ensures that the maximum scallop height (the difference between the machined surface and the designed surface) is minimized. However, this approach does not consider minimizing the cycle time or the material waste, and is sensitive to small curvature changes in the target surface. Chen et al. (2003) select the spatial orientations of passes in multiple flat patches to maximize paint uniformity near the boundaries shared between the patches. Their work does not consider curved surfaces, or the impact of spatial orientation of passes on cycle time and paint waste.

2.1.2. Speed Optimization

Given the spatial location of a coverage path, Ramabhadran and Antonio (1997) present a framework for efficiently optimizing the speed profile of the coverage path. For a specified average paint thickness, they consider two different problems for optimizing the end-effector speed: minimization of the painting time subject to lower bounds on speed, and minimization of the variation in coating thickness. Both these problems are set up as constrained quadratic programs. Their approach does not consider any bounds on end-effector acceleration or upper bounds on end-effector speed. Kim and Sarma (2003) develop a speed optimization model for coverage path generation framework based on vector fields. Their approach determines the end-effector speed along a pass as the maximum end-effector speed allowed by actuator joint and torque limits, thus minimizing the time required by the end-effector to sweep each pass in the path. This approach is suitable for CNC machining, where the surface finish of the machined surface is independent of the end-effector speed, and it is desired to minimize the machining time. However, for spray painting applications, the end-effector speed has a significant impact on the uniformity of paint deposition. Therefore, it is necessary to vary the end-effector speed along the coverage trajectory in a way that ensures that resultant paint thickness is acceptably uniform.

2.1.3. Index Width Optimization

Most prior efforts that optimize the uniformity of material deposition and removal focus on determining the optimal spac-
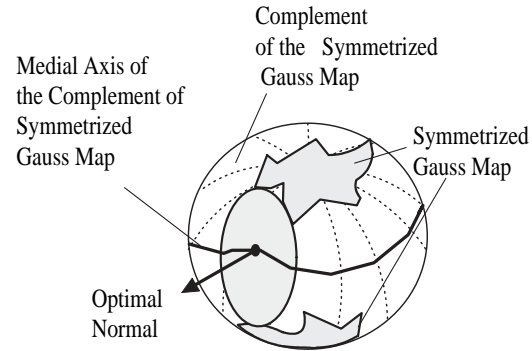

Fig. 4. Smith et al. (2002) determine the optimal section normal as the center of the largest circle inscribed in the complement of the symmetrized Gauss map of the surface.

ing between the adjacent passes. For CNC milling applications, Suresh and Yang (1994) derive the optimal spacing between adjacent passes for a ball-end milling tool. Sarma and Dutta (1997) extend this derivation to desired distributions of scallop height, including the constant scallop height distribution. Determining the optimal inter-pass spacing for robotic spray painting is relatively more involved due to the complexity of the paint distribution flux coming out of the spray gun (Conner et al. 2004). However, most prior path planning approaches consider simplistic deposition models such as circular (Suh, Woo, and Noh 1991), parabolic (Sheng et al. 2000; Freund, Rokossa, and Roßmann 1998; Chen et al. 2002), or beta distributions (Sahir and Balkan 2000). Likewise, most of these approaches make first-order approximations to the surface geometry, thus limiting their use for realistic auto surfaces. Under these assumptions, the selection of index widths between adjacent passes is easier (Suh, Woo, and Noh 1991; Asakawa and Takeuchi 1997; Sahir and Balkan 2000; Sheng et al. 2000; Smith et al. 2002; Chen et al. 2003; Kim and Sarma 2003), but fails to capture the realistic scenario.

Finally, commercially available path planning systems, such as RobCAD™[3] project a user-specified planar path onto the target surface. Simple simulation tools then estimate the output characteristics of the resultant coverage path. The limited specification of the deposition model and the requirement for manual specification of the coverage path limit the utility of such software tools.

2.2. Our Prior Work: Deposition Modeling

In automated path planning systems, it is necessary to effectively determine the suitability of a given coverage trajectory. Therefore, it is desirable to have a paint deposition model that

---

3. A product of Tecnomatix Technologies Ltd.

can predict, with a reasonable accuracy, the paint deposition on an arbitrary surface for a given coverage trajectory. In Conner et al. (2004), we develop a simple model that provides a significant improvement in paint prediction over earlier models while retaining sufficient tractability for use in our planning tools. The deposition model captures the shape of the paint distribution from a spray gun in an analytical representation. The deposition model is composed of one bivariate and two revolved Gaussians (Conner et al. 2002, 2004). We extract the parameters for the deposition model by applying data fitting techniques to the experimental data obtained by painting flat panels (see Figure 3). We then determine the deposition at any point on a given arbitrary curved surface by using the area magnification concept from differential geometry (see Figure 5).

Our geometric deposition model assumes that paint particles flow along polynomial curves after leaving the spray gun nozzle (Conner et al. 2004). While this assumption is not completely accurate, our experience shows us that the assumption is reasonable for surfaces with low curvature. We would like to emphasize that although deposition models are required by the planning procedure, the coverage planning procedures we develop in this work are independent of the particular deposition model used.

3. Seed Curve Selection

Seed curve selection impacts two important output criteria: uniformity of paint deposition and the cycle time. As mentioned in Section 1, the paint deposition uniformity can be seen as having two components: one along the direction of the pass, and the other in the direction orthogonal to the pass. To ensure that the spray gun deposits equal amounts of paint on each side (that is, left and right sides) of the pass and thus produces consistent paint profiles in the direction of the pass, the end-effector should travel along a "straightest" pass, or ideally a geodesic curve (see Figure 6). Therefore, we restrict the set of candidate seed curves to geodesics.

The choice of the seed curve as a geodesic reduces the seed curve selection problem to one that includes only two variables: (1) the spatial orientation of the seed curve, and (2) the relative position of the seed curve with respect to the surface boundary. Note that to increase the likelihood of uniform paint deposition, we must minimize the geodesic curvature on not only the seed curve but also the rest of the offset passes. On surfaces with zero Gaussian curvature (e.g., planar or extruded surfaces), the offset of a geodesic curve is also a geodesic. Therefore, in such cases, the relative position of the geodesic seed curve with respect to the surface boundary has no effect on the geodesic curvature of the resultant offset curves. Then, the relative position of the seed curve with respect to the surface boundary can be picked arbitrarily.

However, on surfaces with non-zero Gaussian curvature (e.g., a sphere), the offset of a geodesic seed curve is, in gen-
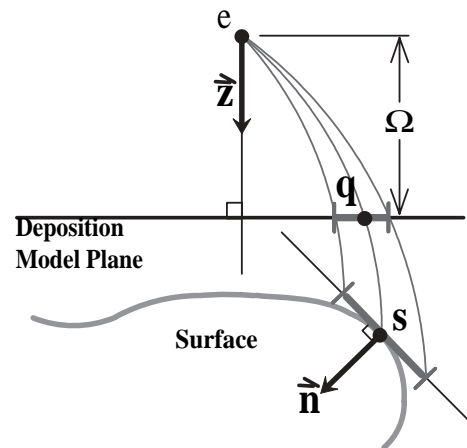

Fig. 5. Our deposition model determines the deposition on any given point on an arbitrary surface using concept of area magnification.

eral, not a geodesic; the geodesic curvature of the offset curve is a function of the surface's Gaussian curvature. On such surfaces, the relative position of the seed curve with respect to the surface boundary has a significant impact on the geodesic curvature of subsequent offset curves, and thus on paint uniformity as demonstrated in Figure 7. In Figure 7(a), the seed curve is selected as a geodesic; however, the offset curves develop high geodesic curvature as they cross the region of high Gaussian curvature near the "vertex" region of the cuboidal surface. In Figure 7(b), the seed curve is a geodesic as well, but it divides the surface symmetrically. Here, the offset passes on both sides of the seed curve develop some geodesic curvature; however, the bending of the resultant offset passes is now significantly reduced, thus improving the likelihood of achieving uniform coverage. This figure demonstrates the impact of the relative position of the seed curve on geodesic curvature of the passes. Therefore, it is desired to select the appropriate position of the seed curve to ensure that the offset curves have minimal geodesic curvature.

In order to examine the effect of the relative position of the seed curve on offset passes, it is convenient to employ the Gauss–Bonnet theorem (Thorpe 1979) and to study the effect of surface Gaussian curvature on the integral of geodesic curvature along a given offset curve (rather than the maximum and minimum values of geodesic curvature). Let us consider a segment C_{st} of the smooth seed curve α_0 (see Figure 8). Let the end-points of C_{st} be $\alpha_0(t_0)$ and $\alpha_0(t_1)$. We will generate an offset curve of C_{st} by measuring the distance between the offset curve and the seed curve along geodesics γ_{t_0} and γ_{t_1} that are orthogonal to the seed curve at points $\alpha_0(t_0)$ and $\alpha_0(t_1)$. Let C_{of} be the offset of C_{st} at an offset distance Δ; we require that
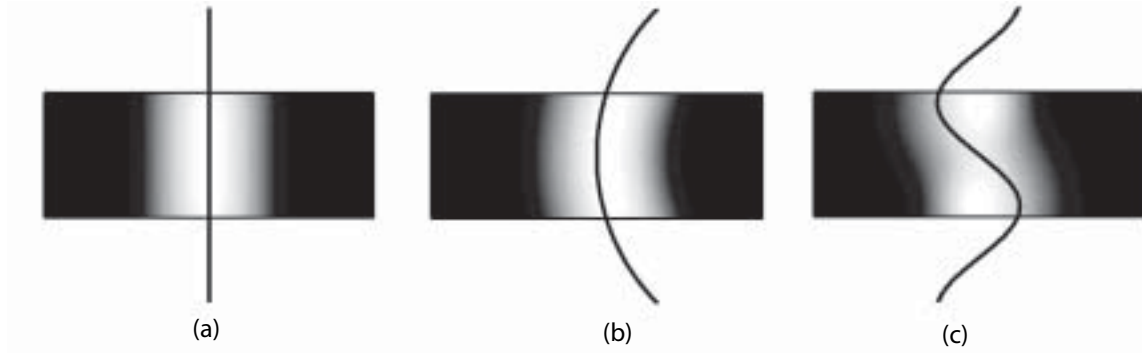
Fig. 6. Effect of geodesic curvature on uniformity of paint deposition. (a) When the pass is a geodesic, i.e., a straight line on the planar surface, there is symmetrical paint deposition on each side of the pass. (b) When the pass has constant non-zero geodesic curvature, i.e., a circular arc, there is more paint deposition on the side towards which the pass bends. (c) When the pass has varying geodesic curvature, the paint deposition on either side of the pass is highly non-uniform.

Fig. 7. (a) The geodesic curvature of offset passes increases as the passes sweep past a region of high Gaussian curvature. (b) If the seed curve (shown as a dark thick curve) splits the surface into two regions with equal integrals of Gaussian curvature, the geodesic curvature of the passes is minimized.

the offset distance Δ is less than the focal length[4] α_0. We are interested in determining the integral of the geodesic curvature along C_{of}. We assume that the surface is C^3 continuous, thus allowing us to assume that C_{of}, γ_{t_0} and γ_{t_1} are all smooth curves.

Let ϕ be the region bounded by C_{st}, C_{of}, γ_{t_0} and γ_{t_1}. Let C_{dia} be any smooth curve joining $\gamma_{t_1}(0)$ and $\gamma_{t_0}(\Delta)$. Denote the surface region bounded by C_{st}, γ_{t_0} and C_{dia} as ϕ_1, and its boundary $\partial\phi_1$ consists of curves C_{st}, γ_{t_0} and C_{dia} with appropriate orientation. Similarly, let ϕ_2 be the region bounded by C_{of}, γ_{t_1} and C_{dia}, and $\partial\phi_2$ be the boundary of ϕ_2.

We first apply the local Gauss–Bonnet theorem to triangular regions ϕ_1 and ϕ_2

$$\int_{\phi_i} K + \int_{\partial\phi_i} \kappa_g = \sum_{j=1}^{3} \theta_{i,j} - \pi, \qquad (1)$$

where K is the Gaussian curvature of the surface ϕ_i, κ_g is the geodesic curvature of the triangular boundary $\partial\phi_i$, and $\theta_{i,j}$ is the jth internal angle of the boundary. Note that C_{dia} is shared by both boundaries $\partial\phi_1$ and $\partial\phi_2$, but is traced in opposite directions. Additionally, the integrals $\int_{\gamma_{t_0}} \kappa_g$ and $\int_{\gamma_{t_1}} \kappa_g$ are zero by definition of geodesics. Therefore,

---

4. If $\alpha_s(t)$ represents a lateral offset of curve α_0 at a distance of s (measured in the surface), the focal length of α_0 is the smallest distance s^* for which the offset curve α_{s^*} self-intersects. Note that at the self-intersection point $\alpha_{s^*}(t^*)$, the magnitude of $\dot{\alpha}_{s^*}(t^*)$ is equal to zero.
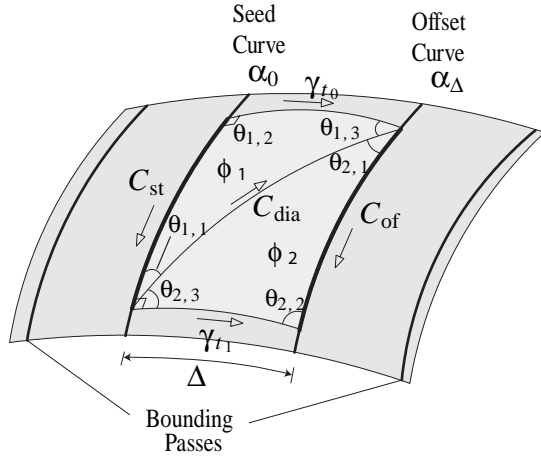
Fig. 8. Application of the Gauss–Bonnet theorem to the region bounded by the seed curve, its offset curve, and the two bounding orthogonal geodesics.

$$\int_{\partial\phi_1}\kappa_g + \int_{\partial\phi_2}\kappa_g = \left(\int_{C_{st}}\kappa_g - \int_{\gamma_{t_0}}\kappa_g - \int_{C_{dia}}\kappa_g\right)$$
$$+ \left(\int_{\gamma_{t_1}}\kappa_g + \int_{C_{dia}}\kappa_g - \int_{C_{of}}\kappa_g\right)$$
$$= \int_{C_{st}}\kappa_g - \int_{C_{of}}\kappa_g. \qquad (2)$$

Clearly, $\int_{\phi_1} K + \int_{\phi_2} K = \int_{\phi} K$. Since geodesics γ_{t_0} and γ_{t_1} are orthogonal to the seed curve, $\theta_{1,1} + \theta_{2,3} = \theta_{1,2} = (\pi/2)$. Also, from Rausch, Wolter, and Sniehotta (1997), the geodesics orthogonal to the seed curve are also orthogonal to the offset curve, that is, $\theta_{1,3} + \theta_{2,1} = \theta_{2,2} = (\pi/2)$. Applying these relations to the summation of eq. (1) applied to regions ϕ_1 and ϕ_2, we arrive at

$$\int_{C_{of}}\kappa_g = \int_{\phi} K + \int_{C_{st}}\kappa_g. \qquad (3)$$

Finally, if the seed curve is a geodesic, then

$$\int_{C_{of}}\kappa_g = \int_{\phi} K. \qquad (4)$$

Equation (4) conveys that the more the surface bounded between the offset curve and the geodesic seed curve bends, the more the geodesic curvature of the offset curves increases. If the sign of the Gaussian curvature remains the same on the surface, we can say that the larger the area bounded between the offset curve and the seed curve, the higher the geodesic curvature of the offset curve will be. Therefore, the possibility of self-intersection is maximal on the bounding passes (see Figure 8). From eq. (4), we infer that in order to minimize the geodesic curvature on the bounding passes, the seed curve should divide the surface into two parts such that the integral of the Gaussian curvature is equal over each part. This approach determines the relative position of the seed curve as defined by a geodesic Gaussian curvature dividing curve.

For a given surface, there are an infinite number of geodesics that are also Gaussian curvature dividers. We wish to choose a seed curve from this family of geodesic Gaussian curvature dividers, such that the cycle time is minimized. Under the assumption that all candidate coverage trajectories yield the same amount of average paint deposition on the surface (through a control of paint flow rate), the portion of cycle time when the spray gun is actually depositing paint on the surface remains approximately constant for all coverage trajectories. As such, the overall cycle time is proportional to the time required for the spray gun to negotiate turns in the path (i.e., when not depositing paint on the surface). Therefore, to minimize cycle time, it is necessary to minimize the number of turns in the coverage path.

To determine the optimal orientation of the seed curve that minimizes the number of turns in the coverage path, we first approximate the geodesic seed curve by a curve of planar intersection that is also a Gaussian curvature divider. Note that if a section plane is orthogonal to the target surface at all points on the resultant intersection, the intersection curve is a geodesic curve. Therefore, to ensure that the seed curve approximation is sufficiently close to being a geodesic, we require that the normal to the section plane be orthogonal to the average target surface normal.

Next, we generalize the concept of surface "altitude" from planar surfaces given by Huang (2001) to non-planar surfaces, where the surface altitude is now measured as the sum of the lengths of the longest orthogonal geodesic curves starting from the seed curve, and extending on either side of the seed curve (see Figure 9). To determine the seed curve, we will select the section plane normal that yields minimal surface altitude. Then, such a choice will result in minimal number of passes in the resultant coverage path, and thus equivalently minimal cycle time and paint waste.

Thus, our seed curve selection procedure simultaneously optimizes the resultant paint deposition uniformity (characterized by passes with low geodesic curvature) and cycle time (characterized by minimal number of turns in the coverage path). In implementation, we first determine the spatial orientation of the seed curve that minimizes the cycle time by selecting the optimal section plane normal. Then, we proceed to select the relative position of the seed curve by determining
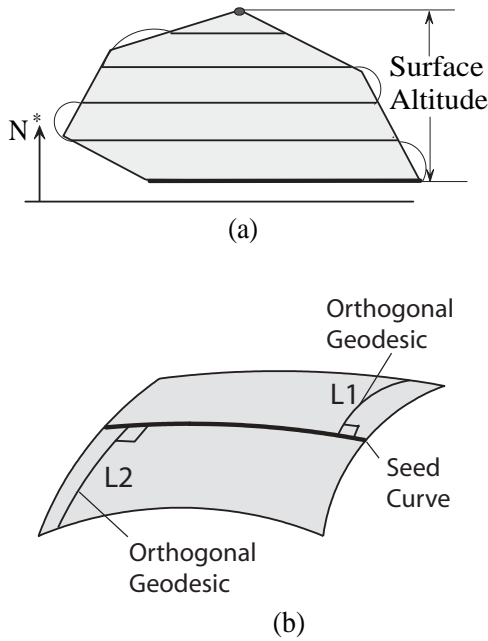
(a)

(b)

Fig. 9. (a) Huang's approach selects the orientation of the passes that minimizes the surface altitude in direction orthogonal to the passes, thus minimizing the cycle time. (b) We extend Huang's approach to curved surfaces by determining the surface altitude as the sum (L1+L2) of the lengths of longest orthogonal geodesics on either side of the seed curve.

the Gaussian curvature divider corresponding to the optimal section plane normal.

4. Speed Optimization

Automotive paint specialists typically use constant speed trajectories. The size of the ESRB deposition pattern is relatively large with respect to a typical automotive surface; therefore, constant speed profiles typically require long oversprays to ensure that the boundary effects, which produce non-uniform paint deposition near surface boundaries, are minimized. If there is a restriction on the maximum acceptable level of paint waste, shorter oversprays must be used, but not without a compromise in the paint deposition uniformity. Additionally, on non-planar surfaces, the changes in the surface curvature along the pass result in non-uniform paint deposition along the pass. Speed optimization attempts to compensate for these curvature related results and improves the uniformity of paint deposition in the direction of the passes (see Figure 10).

Unlike prior approaches (Ramabhadran and Antonio 1997; Kim and Sarma 2003) that use speed optimization techniques over the entire path, our approach uses a semiglobal (i.e., not local, and not entirely global either) method that optimizes
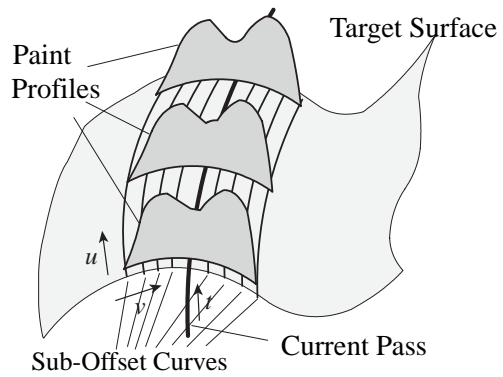

Fig. 10. Speed optimization attempts to minimize the variation of paint profiles in the direction of the pass.

speed profiles on a pass-by-pass basis. The underlying assumptions in our approach are that the speed optimization improves the uniformity in the direction of the passes, and the average paint deposition along a given pass remains constant for any candidate speed profile along that pass. Then, under these assumptions, we have observed that for most surfaces, a local change in the speed profile along a pass affects the paint deposition uniformity on only a subset of the surface surrounding the pass; thus making the scope of our optimization approach semiglobal.

Our objective here is to find a speed parametrization of the pass that minimizes the standard deviation of paint deposition in the direction of the pass. Denote by the set $\hat{s} = \{s(t) : 0 \leq t \leq T\}$ a candidate parametrization of the pass, thus implicitly representing a candidate speed profile $\mathrm{d}s(t)/\mathrm{d}t$. Here, T is the time required for the atomizer to cover the pass at the nominal speed and will be the same for any candidate speed profile along the pass. Let the surface surrounding the given pass be parametrized as a uv patch, where the iso-curves of v represent the suboffset curves (i.e., regular offset curve, but not a part of the coverage path) spaced at distance v from the pass. Let $\alpha_v(u)$ represent a unit-speed parametrization of a suboffset curve.

If $\phi[\alpha_v(u), s(t)]$ gives the paint deposition flux at point $\alpha_v(u)$ when the spray gun is at $s(t)$, the total paint deposition at $\alpha_v(u)$ is given by

$$\mathrm{d}\left(\alpha_v(u), \hat{s}\right) = \int_0^T \phi[\alpha_v(u), s(t)] \, \mathrm{d}t. \tag{5}$$

The average paint deposition, $\bar{d}_v$, is given by

$$\bar{d}_v = \int_{\alpha_v} \frac{\{d\left[\alpha_v(u), \hat{s}\right]\}}{l_v} \, \mathrm{d}u, \tag{6}$$

where l_v is the length of the suboffset curve $\alpha_v(u)$.

Then, the variation of the deposition along $\alpha_v(u)$ is given by

$$\mathsf{var}_v\left(\hat{s}\right) = \int\limits_{\alpha_v} \frac{\left\{ d\left[\alpha_v(u), \hat{s}\right] - \bar{d}_v \right\}^2}{l_v}\, \mathrm{d}u. \qquad (7)$$

Thus, our objective function, i.e., the standard deviation of the paint deposition in the direction of passes is

$$\Upsilon(\hat{s}) = \int\limits_{-v_o}^{v_o} \sqrt{\mathsf{var}_v\left(\hat{s}\right)}\, \mathrm{d}v, \qquad (8)$$

where v_o is the nominal width of the deposition pattern.

Finally, the speed optimization problem is formulated as

$$\min_{\hat{s}} \Upsilon(\hat{s}) \qquad (9)$$
$$\text{such that} \quad v_{min} \leq \tfrac{ds(t)}{dt} \leq v_{max} \quad \forall\, t \in [0, T],$$
$$a_{min} \leq \tfrac{d^2 s(t)}{dt^2} \leq a_{max} \quad \forall\, t \in [0, T],$$

where v_{min} and v_{max} are the velocity limits and a_{min} and a_{max} are the acceleration limits as dictated by the paint process parameters and the robot joint speed/acceleration limits.

In implementation, we solve eq. (9) using a quadratic optimization program with linear constraints by appropriately discretizing the spray gun pass, the sampling of the suboffset curves, and the suboffset curves themselves. In theory, it is possible to obtain an exact optimal solution that minimizes the objective function by using calculus of variations; however, the complex form of the objective function (a triple integral) and the presence of the speed and acceleration constraints limit the scope of determining solutions using calculus of variations on a wide class of surfaces. We examine the effectiveness of our speed optimization formulation in Section 6.2 on a few test surfaces.

5. Index Width Optimization

Once we have optimized the end-effector speed to produce acceptable paint uniformity along the direction of a pass, we focus on how to place passes next to one another on the surface; that is, select index widths between the passes. Given the position of the seed curve, the objective is to select the positions of the rest of the passes in the coverage path by optimizing index widths such that the paint profiles of adjacent passes overlap appropriately and produce acceptable uniformity orthogonal to the direction of the passes. At the same time, the index widths should be as wide as possible in order to reduce the number of passes in the coverage path, thereby reducing the cycle time and paint waste. Therefore, our index optimization procedure seeks to determine the set of index widths between adjacent passes that minimizes a combination of the two costs: (i) the normalized standard deviation of paint deposition over the surface, and (ii) the number of

turns in the coverage path. Additionally, to ensure that the paint deposition is acceptably uniform, we explicitly require that the normalized standard deviation of paint deposition is below the maximum allowable limit. Next, we present procedures to obtain solutions for the index width optimization on surfaces with increasing geometric complexity: planar surfaces, extruded surfaces, and surfaces with non-zero Gaussian curvature.

5.1. Determining Index Widths on Planar Surfaces

On a planar surface, geodesics are simply straight lines. Therefore, the seed curve, chosen as described in Section 3, will be a straight line. The offsets of the seed curve are parallel straight lines and accordingly the resultant coverage path consists of a family of parallel lines. Moreover, for any such straight pass, the planar surface is locally isometric everywhere (ignoring boundaries of the surface). This local isometry of the surface leads to recurring isometric paint profiles as we move along the direction orthogonal to the passes. From this recurring isometry of the paint profiles, it is intuitive that the optimal solution to the index optimization problem yields the same index width between any two adjacent passes.

This assumption of constant optimal index width between adjacent passes enables us to examine the effect of index width on paint deposition uniformity (see Figure 11; Conner et al. 2002). To evaluate paint uniformity, we consider the interactions between the deposition profile curves of a sufficiently large number of passes spaced at constant index width.

From the graph, we observe that there is a "sweet spot" of index width that corresponds to a local minimum of the standard deviation (around 525 mm index width for the atomizer whose deposition pattern was considered in Figure 11). Painting the target surface at this higher index width is desirable because higher index widths lead to a fewer number of turns in coverage path, and thus smaller process cycle time. This corresponds to the minimization of the objective function in our index optimization problem, as mentioned earlier in this section. Unfortunately, the sensitivity of the standard deviation of paint deposition to the index width is high at the sweet spot; in other words, small changes in index width at the sweet spot produce high variations in paint deposition uniformity. In order to ensure that the paint deposition uniformity over the surface is not sensitive to small changes in index width, we typically do not use the sweet spot spacing between the passes. To ensure that the index optimization procedure avoids the sweet spot, we restrict the search of index widths to a closed interval termed the "index width search range", which excludes the sweet spot. In implementation, this search range in discretized at an appropriate resolution.

Thus, for planar surfaces, the index optimization procedure selects the optimum index width as the largest index width in the index width search range that yields an acceptable uniformity. As mentioned earlier, since the planar surface is
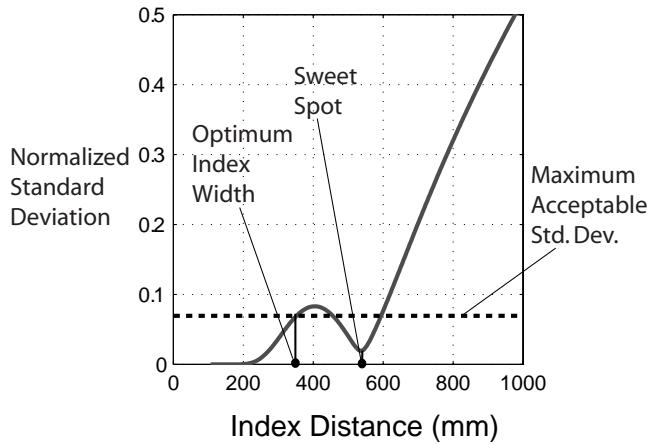
Fig. 11. Graph of normalized standard deviation of paint deposition versus the index width for a typical ESRB deposition pattern.
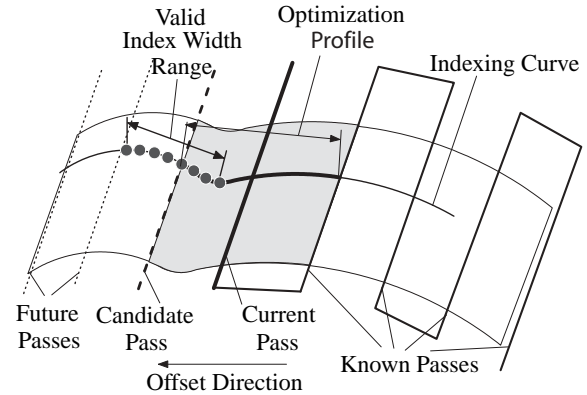

Fig. 12. Index width optimization on extruded sheets: the paint deposition uniformity is calculated along the indexing curve bounded between the previous pass and the candidate pass.

isometric to itself everywhere, the same optimum index width is chosen for all passes, assuming that there is sufficient overspray.

5.2. Determining Index Widths on Extruded Sheets

To lift the index width selection framework from planar surfaces to non-planar surfaces, we first consider a special class of surfaces – extruded sheets. Extruded surfaces have zero Gaussian curvature, yet are non-planar in general. Many automobile surfaces, such as doors, are designed based on extruded surfaces, making this a useful class of surfaces to consider.

Although different choices of seed curve orientation are available on the extruded surface as described in Section 3, for clarity of presentation, we assume that the passes are along the zero curvature direction (see Figure 12). Thus, the surface curvature orthogonal to each pass varies from pass to pass. In general, the paint profiles along any two passes on an extruded surface are different due to the variation in surface curvature. As a result, the optimal spacing between passes varies as surface curvature changes.

Our path planning approach generates new passes by first computing the optimal index width between a known pass and its adjacent pass, and then laterally offsets the known pass within the surface. At the beginning of the trajectory generation procedure, only the seed curve is known and we determine its adjacent passes. The newly generated passes are also categorized as known passes and the process of generating new passes from the most recently generated known pass continues until the surface is covered completely. For the sake of clarity, at a given instance of time, we term the known pass we are considering the "current pass".

Then, the resulting paint deposition uniformity in the surface region surrounding the current pass depends on the cumulative deposition due to the set of the known passes, K, (including the current pass) as well as a set of future passes, F, whose locations are unknown at the moment. For typical ESRB atomizers, it is sufficient to consider the deposition due to three or four future passes because future passes that are farther away from the current pass have negligible paint deposition near the region surrounding the current pass.

To determine the optimum index width, w_{cur}, between the current pass and its next adjacent pass (i.e., the first future pass), we vary the position of the next three or four future passes such that the spacing between the adjacent passes lies in the index width search range. We then evaluate the paint deposition uniformity on the optimization profile curve bounded between the current pass and its adjacent future pass (see Figure 12). We denote by $\mathsf{var}(F, K)$ the normalized standard deviation of paint deposition due to the known passes and the selected future passes, measured on the optimization profile curve bounded between the current pass and the first future pass. The sets of future passes that yield acceptable paint uniformity over the selected optimization profile are categorized as the set of feasible index widths.

Then, the index width optimization problem for the extruded surfaces is formulated as

$$\min_{w_{cur}} f\left[\mathsf{var}(F, K), \frac{L}{w_{cur}}, (w_{cur} - w_{prev})\right] \quad (10)$$

$$\text{such that} \qquad \mathsf{var}(F, K) < \mathsf{var}_{max}$$

$$F_i \in \mathcal{SR} \quad \forall i,$$

where f is the objective function (monotonically increasing in its arguments), L is the altitude of the surface for the given seed curve, w_{prev} is the index width between the current pass

and its adjacent known pass, F_i represents ith element of set F, and $\mathcal{SR}$ is the index width search range.

Note that the cost component associated with quantity $(w_{cur} - w_{prev})$ in the objective function ensures an appropriate balance between the deposition on the region between the current pass and the previous pass, and the deposition on the region between the current pass and the candidate pass. Then, the index width from the set of future passes that yields the minimal cost is chosen as the optimum index width, and accordingly the new candidate offset pass is generated.

5.3. Determining Index Widths on Surfaces with Non-zero Curvature

On surfaces with non-zero Gaussian curvature, the curvature of the surface, in general, changes not only as we move along an indexing curve (as in the extruded surface case), but also as we move along a given pass. As such, the geometry of the indexing curve (i.e., the curve orthogonal to start curve) changes as we move along a given pass. Here, in order to determine the offset of the current pass, we sample the current pass at a finite number of "marker" points spaced at intervals based on the total curvature of the pass. At each marker point, we then determine the indexing curve as the intersection curve of a plane whose normal is along the tangent to the pass at that marker point. We determine the optimum index width along each indexing curve and obtain the corresponding offset marker point by tracing along the indexing curve a distance equal to the optimum index width from the current marker point. The offset curve is then determined by interpolating between the collection of offset marker points.

To determine the optimum index width at each marker point, we first approximate the surface locally with a surface of extrusion generated by extruding the indexing curve along the direction tangent to the pass at the marker point (see Figure 13). Employing the same approach used for the extruded sheets, we then determine the set of feasible index widths, $\mathcal{F}^i$, on the extruded surface approximation at each marker point i. For l marker points, we construct index sets formed by a combination operation by picking a single element from each $\mathcal{F}^i$ at a time. That is, an index set is represented as $\mathcal{I} = \{w^1, w^2, ..., w^l\}$, where $w^i \in \mathcal{F}^i$. Note that each index set, formed by choosing a different combination of elements from each $\mathcal{F}^i$, represents a different offset curve.

For each index set, we calculate the objective function as the summation of the objective function for extruded surface approximations at each marker point (i.e., $\sum_i f_i$, where f_i is the objective function for the extruded surface approximation at marker point i as described in eq. 10), and an additional component that collectively measures how much the candidate index width at each marker point differs from those at the neighboring marker points. This additional component of the cost function favors index sets that have the same candidate index widths at all marker points, and thus implicitly attempts
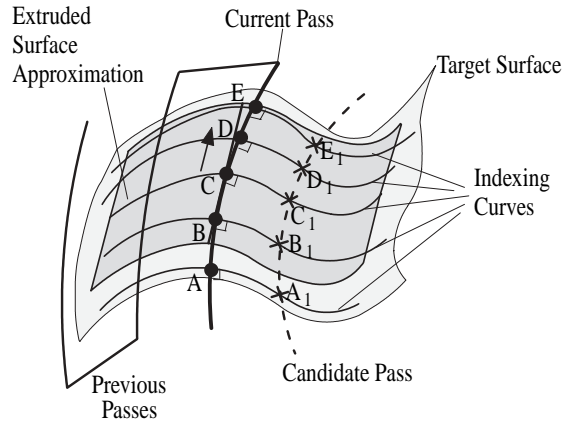

Fig. 13. Index width optimization on arbitrary surfaces. At each of marker point A, B, C, D, and E, we approximate the surface with an extruded surface using the indexing curve, and determine the uniformity graph along the indexing curve. A_1, B_1, C_1, D_1, and E_1 are the corresponding offsets of the marker points.
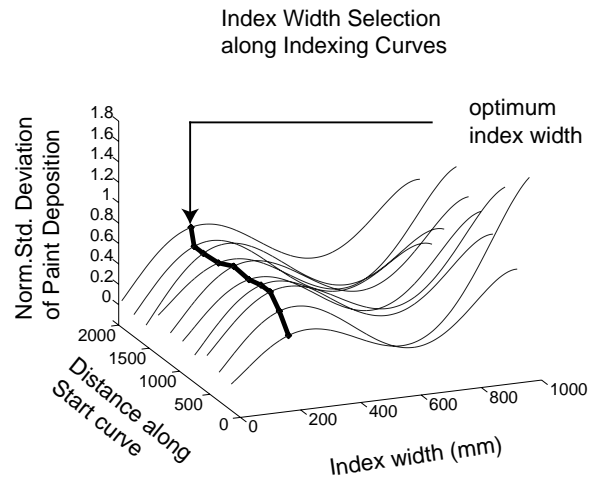

Fig. 14. Index width optimization on arbitrary surfaces. The optimization procedure determines the optimum index width at each marker point for surface shown in Figure 13.

to minimize the geodesic curvature of the offset curve. Then, by constructing all index sets and evaluating the associated objective function for each index set, the optimal index set can be identified and correspondingly the adjacent offset curve can be determined.

In implementation, instead of considering all possible index sets, our approach considers only those index sets which

represent the same index width at all marker points. That is, we restrict the search for the next offset curve to only those which maintain a constant spacing from the current pass at all marker points. Such a restriction not only allows us to quickly determine a good solution to the index width optimization problem, but also implicitly reduces the possibility of subsequent offset passes developing self-intersections. Moreover, this optimum "constant index set" solution can serve as the starting point for a gradient-descent based method that operates in the search-space of all possible index sets for further improvement in uniformity.

6. Simulation and Experimental Results

To validate the utility of our seed curve selection procedure, we compare the simulation results for coverage paths constructed using our method to a method based on the Gauss map (Smith et al. 2002). Similarly, to examine the effectiveness of our speed and index optimization procedures, we generate spray gun trajectories using our planning tools on a variety of simple surfaces and study the effects on paint deposition uniformity. To evaluate paint deposition uniformity corresponding to the generated trajectories, we simulate the paint deposition process on corresponding surfaces using the paint deposition model described in Conner et al. (2004). All paint simulations discussed in this paper assume that the paint particles flow along polynomial curves. Next, we experimentally measure the paint uniformity on some real automobile surfaces.

The surfaces used for verification of our planning tools have varying geometric complexity including planar sheets, cylindrical surfaces, a door panel from a Ford Excursion and a fender from a Ford Crown Victoria. We model each of the two automobile surfaces by a single C^2-continuous NURBS surface that is slightly simplified by removing holes and merging multiple NURBS patches together from the corresponding CAD data. We then generate trajectories on the corresponding approximation surfaces, and use these same trajectories for experimentally painting the surfaces and for simulating paint deposition on the surface CAD models (see Figure 17).

6.1. Seed Curve Selection

Our procedures determine the seed curve as a curve of planar intersection such that it is a Gaussian curvature divider and also minimizes the number of turns in the coverage path. We compare the effectiveness of our seed curve selection procedure with the Gauss map modified (GMM) procedure closely related to the method used by Smith et al. (2002), which selects the seed curve using a section plane that is maximally orthogonal to the target surface. In other words, the section plane normal computed by the GMM approach corresponds to the center of largest circle inscribed in the complement of the symmetrized Gauss map of the surface. For a meaningful comparison between the two approaches, the relative position of the seed curve in the GMM approach is selected such that the seed curve is also a Gaussian curvature divider. For both these approaches, coverage trajectories are then generated using the trajectory generation algorithm described in this paper, except that the index width between any two adjacent passes is kept constant.

The test surfaces used by Smith et al. (2002) are very small compared to the width of spray gun deposition pattern. To have realistic paint deposition scenarios, we scale surface 2 described in Smith et al. (2002) by a factor of 1000/2.54 (see Figures 15(a) and 15(b)). In Table 1, we compare (in simulation) the output characteristics obtained by employing our method to those of the GMM method. On a scaled version of surface 2 described in Smith et al. (2002), our method yields a 20% relative improvement in deposition uniformity, where we measure the uniformity in terms of normalized standard deviation of paint deposition. Also, there is a relative improvement of 16.66% in cycle time (measured in terms of number of turns).

We also compare the two seed curve selection approaches for more realistic auto body surfaces, e.g., a surface approximating the surface of a Ford Crown Victoria front side fender (see Figure 16). For this fender-resembling surface, our method yields normalized standard deviation for paint equal to 10.18%, where the resultant coverage path is free from self-intersections. The coverage path constructed using the GMM method yields higher normalized standard deviation of paint deposition at 13.08%. Additionally the coverage path has self-intersections, thus making the end-effector motion practically infeasible. For this fender surface, our method gives the number of turns in the coverage path equal to six, where as for the GMM method it is nine. Thus, our seed curve selection improves not only uniformity but cycle time also.

6.2. Speed Optimization Results

To examine the improvement in the resultant paint deposition uniformity using speed optimized trajectories over constant speed trajectories, we evaluate the resultant paint uniformity in each case over a few surfaces and list the results in Table 2. We measure the uniformity in terms of normalized standard deviation of paint deposition. The results show that in

Table 1. Comparison of our Method to GMM Approach

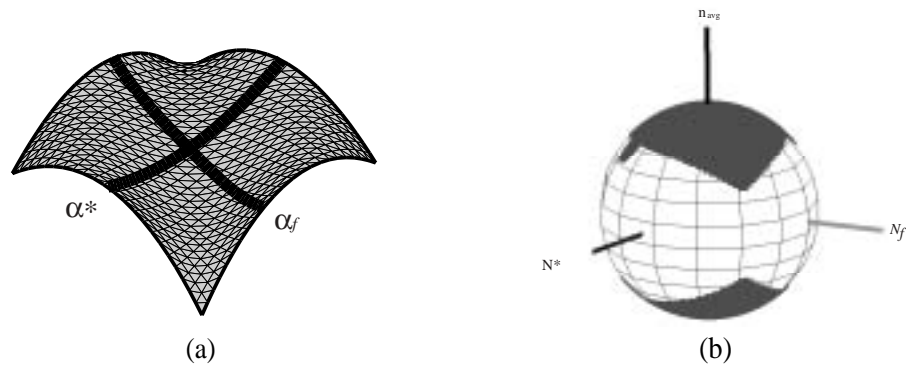| Test Surface	Proposed Approach		GMM Method	
	Std dev	Turns	Std dev	Turns
Surf #2	11.34%	12	13.67%	14
CV fender app	10.18%	6	13.08%	9

(a)   (b)

Fig. 15. (a) On a scaled version of surface 2 from Smith et al. (2002), α^* is the Gaussian curvature divider seed curve determined by our approach. The spatial orientation of α^* is obtained as the intersection a section plane with optimal normal $\mathbf{N}^*$ that minimizes the number of turns in the coverage path. The GMM approach, based on the Smith et al. method, determines the curve α_f as the seed curve. The spatial orientation of α_f is along the intersection of a maximally orthogonal section plane (with normal N_f). (b) Symmetrized Gauss map for the surface; $\mathbf{n}_{avg}$ is the average surface normal. Note that although N_f and $\mathbf{N}^*$ are orthogonal to the surface normal, their spatial orientations are significantly different. $\mathbf{N}^*$ is not maximally orthogonal to the surface; however, it minimizes the number of turns in the coverage path.
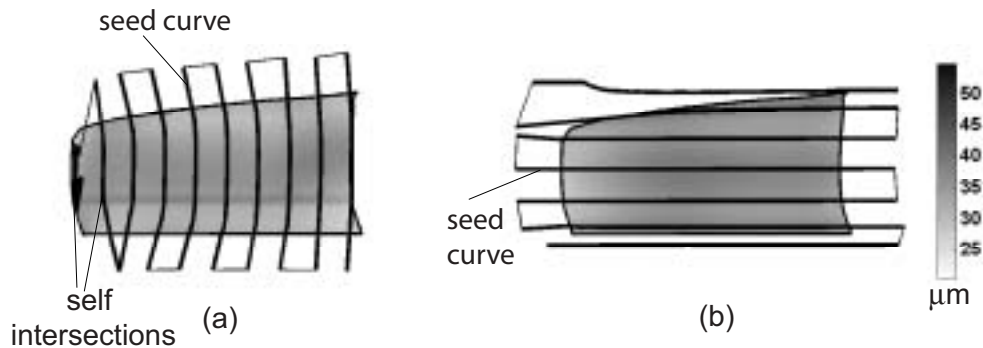

Fig. 16. Seed curve selection on a surface approximating the Crown Victoria fender. (a) The trajectory generated using GMM approach has self-intersections near the high curvature region on the left side of the fender. (b) Our approach yields trajectory free from self-intersections and simultaneously minimizes number of turns in the path.

simulation, the speed optimization substantially improves the uniformity of resultant paint deposition. Also, the planar surface example shows that to produce similar uniformity, the overspray required by the speed optimized trajectories is shorter than that required by a constant speed trajectory.

To examine the effectiveness of our trajectory planning system, we performed a number of experiments on the Ford Excursion door in a paint booth. The door was mounted on a vertical rectangular board which was bigger in size than the door. The door was painted using a single ABB S3 robotic

manipulator fitted with a 50 mm ABB Micro-Micro Bell atomizer.

The experimental data on the Ford Excursion door show that the speed optimized trajectory (15.88% normalized standard deviation; see Figure 18) yields an improvement in the paint deposition uniformity over a constant speed trajectory (17.80% normalized standard deviation); however, the relative improvement in uniformity due to speed optimization is small. This relatively small improvement in uniformity is attributed to the fact that the simulation paint deposition differed

Table 2. Impact of Speed Optimization on Normalized Standard Deviation of Paint Deposition

	Simulation	
Surface	Const. Speed	Optimized
Excursion door	21.82 %	15.73 %
Approx. to Crown Victoria fender	16.62 %	11.92 %
Plane 100mm overspray	8.60 %	3.88 %
Plane 235mm overspray	3.88 %	-

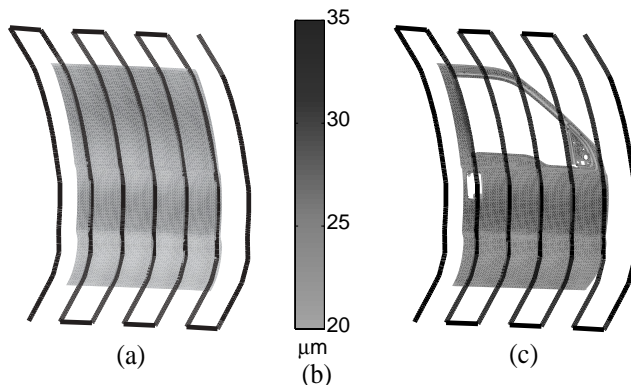Fig. 18. A typical optimized speed profile along a spray gun pass.

Fig. 17. (a) Simple surface approximation to the Ford Excursion door and the resultant paint deposition on the surface. (b) The color map shown is specifically designed to bring out the paint deposition variation. (c) Once the path on the approximation surface is generated, we simulate the paint deposition on the CAD model of a Ford Excursion door.

Table 3. Index Width Optimization Simulation Results

Target Surface	Normalized Standard Development (%)
Planar Sheet	2.64%
100 cm Radius Cylinder passes parallel to axis	2.21%
100 cm Radius Cylinder passes around cylinder	4.19%
Approximation to Ford Excursion Door Passes along zero curvature direction	6.81%
Approximation to Ford Excursion Door Passes along max. curvature direction	4.48%
Approx. to Crown Victoria fender	11.92%

from the measured paint deposition by as much as 30% (near regions of high curvature) for the Excursion door (Conner et al. 2004). The effectiveness of speed optimization inherently relies on accurate simulation of paint deposition; and more realistic deposition models will enable the speed optimization procedure to significantly improve the uniformity in real systems.

6.3. Index Width Optimization Results

To study the effect of index width optimization on paint deposition uniformity, we consider a variety of target surfaces, generate passes for each of them and evaluate the paint deposition uniformity by simulating the paint deposition process (see Table 3). In each case, we set the maximum allowed normalized standard deviation at 4% and assume sufficient overspray is available to minimize the boundary effects. We observe that the index optimization yields the desired uniformity in cases where the surface curvature remains constant along the index-
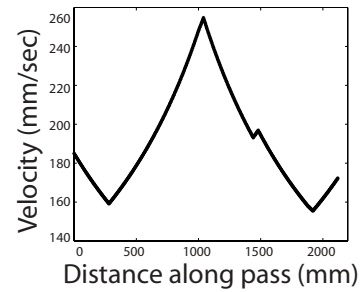
ing curve. On the other hand, if the surface curvature changes along the indexing curve as in the case for the Ford Excursion (with passes along zero curvature direction) and the Ford Crown Victoria fender, the normalized standard deviation of paint deposition from the obtained trajectory exceeds the desired level. The higher standard deviations observed on these surfaces reflect the fact that the index optimization process is semiglobal in nature, and does not necessarily yield globally optimal solutions.

We also studied the effect of index optimization on paint uniformity experimentally by painting the middle and lower portion of a Ford Excursion door with similar settings used for the speed optimization tests. During the experiments, our planning tools generated the index optimized path with a sideways overspray pass near the door bottom. In simulation, this path yielded a paint deposition uniformity of 7.16% on the door. However, because of robot workspace constraints, we had to manually remove the bottom overspray pass from the coverage path. For the coverage path without the overspray

pass, the uniformity of resultant paint deposition was 13.13% in simulation, whereas experimentally it was measured to be 16.5%. If we optimize the index width with the constraint that there would be no bottom overspray pass, the resultant paint deposition uniformity can be improved to 9.01% in simulation. Thus, our planning tools perform with limited success when there is a constraint on use of overspray passes. None the less, our procedures yield desired uniformity results (when sufficient overspray is available) in a reasonable amount of time, and can offer guidelines to the paint specialists to substantially reduce the robot programming time.

7. Conclusion

In this paper, our approach examines the relationship between the variables and the output characteristics of the uniform coverage problem on simple yet realistic surfaces. We then decompose the coverage problem into three relatively independent subproblems, thus significantly reducing the dimensionality of the search space for the coverage problem. This dimensionality reduction enables us to solve the coverage problem in a reasonable amount of time without overtrivializing assumptions about the deposition pattern or the surface geometry. Although we consider the deposition models only for ESRB atomizers, our coverage procedure is independent of the deposition model and can be used for any other type of deposition patterns.

By taking a recourse to the Gauss–Bonnet theorem from differential geometry, we are able to identify the interaction between the surface curvature and the geodesic curvature of the passes in the coverage path. This understanding enabled us to develop a seed curve selection procedure that improves both paint deposition uniformity and cycle time compared to previous approaches.

The simulation results from the index-optimized and speed-optimized trajectories show that, in the presence of sufficient overspray, the subproblems of speed optimization along the passes and the index width optimization remain relatively independent. Simulation results indicate that by optimizing the end-effector speed along the passes, paint uniformity improves by more than 25% (relative, and compared to constant speed trajectories) on the test surfaces. Given sufficient overspray, the simulation results for index width optimization tests show that in cases where the surface is symmetrical in the direction orthogonal to the passes, the planned trajectories meet the desired uniformity goals; whereas in other cases, the resultant uniformity is higher than desired.

In the absence of sufficient overspray, deposition constraints in the speed optimization problem may impact the index optimization results adversely, thus producing nonuniform paint deposition near surface boundaries. In such cases, optimization of the end-effector speed along the entire trajectory can significantly improve paint deposition uniformity.

Segmentation of the automobile surface into geometrically as well as topologically simple subsets is an important step in our trajectory generation framework. Such a segmentation of the surface enables us to apply the trajectory generation procedures described in this paper to each of the resultant segment. Then, by joining the obtained trajectories appropriately, the entire surface can be covered completely and uniformly, thus bringing us closer to a turn-key automated trajectory generation system for automobile surfaces. Our future work will address these issues to extend the path planning algorithm to a broader class of surfaces.

Acknowledgments

References

Asakawa, N. and Takeuchi, Y. 1997. Teachless spray-painting of sculptured surface by an industrial robot. *Proceedings of the IEEE International Conference on Robotics and Automation*, Albuquerque, NM, April, Vol. 3, pp. 1875–1879.

Atkar, P. N., Conner, D. C., Greenfield, A., Choset, H., and Rizzi, A. A. 2005. Hierarchical segmentation of surfaces embedded in $\Re^3$ for auto body painting. *Proceedings of the IEEE International Conference on on Robotics and Automation*, Barcelona, Spain, April.

Chen, H., Sheng, W., Xi, N., Song, M., and Chen, Y. 2002. Automated robot trajectory planning for spray painting of free-form surfaces in automotive manufacturing. *Proceedings of the IEEE International Conference on Robotics and Automation*, Washington, DC, May, Vol. 1, pp. 450–455.

Chen, H., Xi, N., Wei, Z., Chen, Y., and Dahl, J. 2003. Robot trajectory integration for painting automotive parts with multiple patches. *Proceedings of the IEEE International Conference on Robotics and Automation*, Taipei, Taiwan, September, Vol. 3, pp. 3984–3989.

Conner, D. C., Atkar, P. N., Rizzi, A. A., and Choset, H. 2002. Deposition modeling for paint application on surfaces embedded in $\mathbb{R}^3$ for use in automated trajectory planning. Technical Report CMU-RI-TR-02-08, Carnegie Mellon, Robotics Institute, Pittsburgh, PA, June.

Conner, D. C., Greenfield, A., Atkar, P. N., Rizzi, A. A., and Choset, H. 2004. Paint deposition modeling for trajectory

planning on automotive surfaces. *IEEE Transactions on Automation Science and Engineering* submitted.

Freund, E., Rokossa, D., and Roßmann, J. 1998. Process-oriented approach to an efficient off-line programming of industrial robots. *Proceedings of the 24th Annual Conference of the IEEE Industrial Electronics Society (IECON '98)*, Vol. 1, pp. 208–213.

Held, M. 1991. *On Computational Geometry of Pocket Machining*, Lecture Notes in Computer Science, Springer-Verlag, New York.

Huang, W. H. 2001. Optimal line-sweep-based decompositions for coverage algorithms. *Proceedings of the IEEE International Conference on Robotics and Automation*, Seoul, Korea, May, Vol. 1, pp. 27–32.

Kim, T. and Sarma, S. E. 2003. Optimal sweeping paths on a 2-manifold: a new class of optimization problems defined by path structures. *IEEE Transactions on Robotics and Automation* 19(4):613–636.

Ramabhadran, R. and Antonio, J. K. 1997. Fast solution techniques for a class of optimal trajectory planning problems with applications to automated spray coating. *IEEE Transactions on Robotics and Automation* 13(4):519–530.

Rausch, T., Wolter, F.-E., and Sniehotta, O. 1997. Computation of medial curves on surfaces. *The Mathematics of Surfaces VII*, Information Geometers, pp. 43–68.

Sahir, M. A. and Balkan, T. 2000. Process modeling, simulation, and paint thickness measurement for robotic spray painting. *Journal of Robotic Systems* 17(9):479–494.

Sarma, R. and Dutta, D. 1997. The geometry and generation of NC tool paths. *Journal of Mechanical Design* 119:253–258.

Sheng, W., Xi, N., Song, M., Chen, Y., and MacNeille, P. 2000. Automated CAD-guided robot path planning for spray painting of compound surfaces. *Proceedings of the IEEE/RSJ International Conference on Intelligent Robots and Systems*, Takamatsu, Japan, October 30–November 5, Vol. 3, pp. 1918–1923.

Smith, T. S., Farouki, R. T., al Kandari, M., and Pottman, H. 2002. Optimal slicing of free-form surfaces. *Computer Aided Geometric Design* 19:43–64.

Suh, S-H., Woo, I-K., and Noh, S-K. 1991. Development of an automated trajectory planning system (ATPS) for spray painting robots. *Proceedings of the IEEE International Conference on Robotics and Automation*, Sacramento, CA, April, pp. 1948–1955.

Suresh, K. and Yang, D. C. H. 1994. Constant scallop height mechining of free-form surfaces. *Journal of Engineering for Industry* 116:253–359.

Thorpe, J. A. 1979. *Elementary Topics in Differential Geometry*, Springer-Verlag, New York.